Spectral wave dissipation over a roughness-varying barrier reef

Damien Sous, Kévin Martins, Marion Tissier, Frédéric Bouchette, Samuel Meulé

Spectral wave dissipation over a roughness-varying barrier reef

Damien Sous[1,2], Kévin Martins[3,4], Marion Tissier[5], Frédéric Bouchette[6], Samuel Meulé[7]

[1]Université de Toulon, Aix Marseille Université, CNRS, IRD, Mediterranean Institute of Oceanography (MIO), La Garde, France
[2]Université de Pau et des Pays de l'Adour, E2S UPPA, SIAME, Anglet, France
[3]Univ. Bordeaux, CNRS, Bordeaux INP, EPOC, UMR 5805, F-33600 Pessac, France
[4]Water Research Laboratory, School of Civil and Environmental Engineering, UNSW Sydney, 110 King Street, Manly Vale, NSW, 2093, Australia
[5]Delft University of Technology, Faculty of Civil Engineering and Geosciences, Delft, The Netherlands
[6]GEOSCIENCES-Montpellier, Univ Montpellier, CNRS, Montpellier, France
[7]Aix Marseille University, CNRS, IRD, INRAE, Coll France, CEREGE, Aix-en-Provence, France

Corresponding author: Damien Sous, `sous@univ-tln.fr`

This article has been accepted for publication and undergone full peer review but has not been through the copyediting, typesetting, pagination and proofreading process, which may lead to differences between this version and the Version of Record. Please cite this article as doi: 10.1029/2022GL102104.

Abstract

The present paper reports on a field experiment performed over a shallow, roughness-varying barrier reef at Maupiti island, French Polynesia. The spectral wave energy balance is examined, outside the breaking zone and accounting for non-linear transfers and mean current, to estimate the wave friction factor. This latter varies from 0.05 to 4, with dependence on the ratio between near-bed orbital amplitude and roughness height well predicted by an adjusted parameterization from Madsen (1995). The present results are discussed with respect to other field data recovered on coral and rocky grounds.

1 Introduction

By promoting mixing, aeration, nutrient transport and water renewal, surface waves are critical for the health of coral reef-lagoon systems. In return, thriving coral reefs play an essential sheltering role to low-lying shorelines, protecting them from wave-driven hazards such as flooding and deleterious erosion. Coral reefs, being fringing or barrier, generally exhibit a striking geometrical complexity and very shallow water depths, which leads to significantly enhanced breaking- and friction-induced wave and momentum dissipation compared to the sandy beach situation (Lowe et al., 2005; Reidenbach et al., 2006; Rosman and Hench, 2011; Monismith et al., 2015; Rogers et al., 2018; Sous et al., 2020a; Davis et al., 2020). A significant research effort has been engaged over the last two decades to better understand and predict the physics of waves and wave-driven processes over coral reefs. An essential issue is to decipher the role of coral-induced drag on the evolution of incident waves, which is fully-coupled with the momentum balance, *i.e.* it both affects and depends on the water level and the current field (Symonds et al., 1995; Hearn, 1999; Gourlay and Colleter, 2005; Monismith et al., 2013; Sous et al., 2020a).

The wave energy dissipation rate by bottom roughness is related to the orbital velocity: shorter and higher waves will experience more dissipation. Depending on the coral canopy height, the depth, the spatial and temporal scales to be resolved and the computational resources, the frictional energy dissipation experienced by incident waves propagating over coral reefs may be represented either in the bottom roughness or in the canopy drag frameworks. While few works have addressed the coral-induced wave dissipation in the canopy framework (Rosman and Hench, 2011; Sous et al., 2020a; Qu et al., 2022; Buckley et al., 2022), the bottom roughness approach remains overwhelmingly used due to its simplicity. It relies on the wave friction coefficient f_w (or the wave energy dissipation factor f_e), knowledge of which is essential in many wave and wave-driven circulation models. Field observations of f_w over coral reefs display a strong variability, with typical values ranging between 0.05 and 0.4 (Lowe et al., 2005; Péquignet et al., 2011) but with much higher values found at specific sites (1 for Acevedo-Ramirez et al., 2021, and even 1.8 for Monismith et al., 2015). This variability in f_w principally originates from the variations in hydrodynamic conditions (waves, depth, mean current) and in the geometrical structure of the coral colony. It is generally assumed that the hydrodynamic conditions can be simply represented by a representative near-bed orbital amplitude A_b and, on the other hand, that the roughness structure can be accounted for by a single length-scale. This latter is either directly the standard deviation of the fine-scale bed elevation σ_b, inferred from high-resolution survey, or the so-called hydraulic roughness height k_r used to build the wave boundary layer theory, which remains to be connected to the roughness statistics. Empirical (Lentz et al., 2016; Gon et al., 2020) or theoretical (Madsen, 1995; Lowe et al., 2005) models relating f_w to A_b/k_r or A_b/σ_b have been confronted with field measurements over coral reefs and rocky shores. While the agreement is generally satisfactory for large orbital amplitude to roughness height ratio, discrepancies have been observed for very large roughness (Lentz et al., 2016; Gon et al., 2020). Another sparsely documented issue is the role played by currents, which are expected to provide additional shear and to increase wave dissipation. A proper assessment of the validity of classical wave-

current bottom drag dissipation (Madsen, 1995) in the coral reef context remains to be done, in particular in open reef systems where wave breaking-driven barotropic currents are ubiquitous.

The parameterization of bottom drag in wave models raises therefore the complex question of the connection between reef topography and hydrodynamics (Davis et al., 2020). Significant efforts have been recently devoted to understand the connection between hydrodynamics and roughness structure, in order to allow an easier and more robust definition of frictional parameters in wave and circulation models without the need to perform costly and site-specific hydrodynamic measurements (Lowe et al., 2005; Lentz et al., 2016; Poate et al., 2016; Yu et al., 2018; Gon et al., 2020; Lavaud et al., 2022). Placed in this global effort, the present paper reports on a field study of frictional wave dissipation over the SW barrier reef at Maupiti Island, French Polynesia. As most barrier reefs found worldwide, cross-barrier currents are mainly forced by waves breaking over the ocean side of the forereef. In addition, this site has the particularity to display a well-marked spatial partition of roughness structure (Sous et al., 2020b,0). With a dedicated instrumentation across the backreef, where wave breaking processes cease, the observations allow to track the response of wave transformation and dissipation to the evolution of reef structure. The presence of large roughness height to depth ratio over the barrier combined with a fully spectral analysis further allows to estimate f_w at small A_b/k_r ratio. Section 2 is dedicated to the description of field experiments and related data processing. Results are presented and discussed in Sections 4 and 5, respectively.

2 Field site and Methods

2.1 Field Site and Experiments

Maupiti ("the Stuck Twins") is a diamond-shaped island located in the western part of the Society archipelago in French Polynesia. The present study focuses on the data recovered over a single cross-barrier transect located in the south-west barrier (Fig. 1A) during the MAUPITI HOE field campaign, from 5 to 18 July 2018. The studied area is representative of the reef structure observed along the 4 km-long southwestern barrier reef, showing an alongshore-uniform structure exposed to swell approaching with weak incident angles and a healthy reef colony. In the cross-barrier direction, the reef displays a clear partitioning of bottom roughness that ranges from low-crested compact structures at the reef crest to higher and sparser coral bommies on the backreef (Sous et al., 2020b). The experimental setup was specifically designed to analyse and to differentiate the dynamics over three roughness-contrasting sections found over the barrier reef.

An array of sensors was deployed along a single cross-barrier transect shown in Fig. 1B and C. Positions along this transect are here defined in an onshore-directed referential, with origin at the 20 m isobath. Except S4, each sensor has been repeatedly positioned by DGPS-RTK. Incident wave conditions were measured by an electro-magnetic current meter S4 deployed on the forereef in 10.5 m depth and recording 20-min bursts of data every 3 h. Five pressure sensors (OSSI-010-003®), namely OSS2 to OSS6, were bottom-mounted across the barrier reef to monitor waves and mean water levels. OSS2 was located at the top of the reef crest while OSS3 to OSS6 sensors were specifically located at the boundaries between the three distinct barrier zones described by Sous et al. (2020b). The bottom pressure was continuously recorded at 10 Hz. An acoustic Doppler profiler AQP1 (Nortek Aquadopp®) was deployed near the seabed 500 m beyond the barrier in order to capture cross-barrier transports. The vertical profiles of current velocities were recorded every 3 s with a vertical resolution of 0.1 m. The recovered data is averaged over five successive profiles, *i.e.* 15 s, and projected into the reef barrier axes to obtain the cross and along-reef components. The measured transport at this location can be used to estimate the depth-averaged current velocities at any location across the barrier by simply dividing the transport by the local depth.

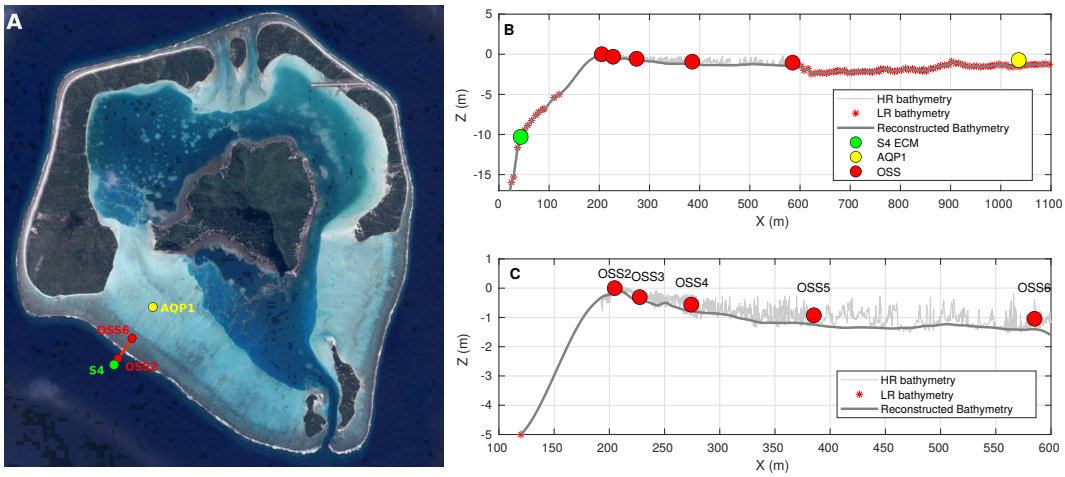

Figure 1. Field site and experimental setup. A: Satellite view of the Maupiti island with the instrumented cross-barrier transect indicated by the red line. B: cross-barrier profile with high-resolution (HR - grey line) and low resolution (LR - red stars) bathymetry data, S4 electro-current meter (green dot), AQP1 Acoustic Doppler velocity profiler (yellow dot) and OSS pressure sensors (red dots). The reconstructed bathymetry is displayed as solid grey line. C: zoomed view of B.

A series of high-resolution topo-bathymetric surveys have been carried out to characterize the detailed geometrical structure of the barrier reef, see Sous et al. (2020b). Profiles P1 and P2 from Sous et al. (2020b), which closely overlap the instrumented transect, are combined to provide high-resolution reef topography denoted in grey dots in Figure 1B and C. The definition of the actual seabed is not straightforward in such complex environment. The approach retained here is based on the analysis of the reef geometrical structure proposed by Sous et al. (2020b). The high-resolution reef topography is processed with a 7 m-wide moving window, corresponding to the fractal saturation threshold observed on the reef elevation spectra (Sous et al., 2020b). In each window, the actual seabed is defined as the 10-th percentile of the reef elevation. This approach ensures to preserve topographical wavelengths larger than 7 m, which are therefore assigned as *bathymetry-related terrain features* (mainly dead substratum), while smaller length-scales associated with living reef colonies are considered as *roughness-related terrain features*.

The bathymetry recovered from the high-resolution reef topography data is completed at both seaward and landward sides by boat soundings carried out during calm days (Fig. 1B and C, red stars). The breaking zone extending from the mid-forereef to the reef crest remaining out of access, the unknown portion of the bathymetry between the on-foot high-resolution reef crest elevation data from Sous et al. (2020b) and the forereef boat sounding performed for the present experiment, has been reconstructed using piecewise cubic interpolation (Fig. 1B and C, thick grey line).

The reef barrier is divided in three successive sections (Sous et al., 2020b), each being monitored by sensor pairs OSS3-OSS4, OSS4-OSS5 and OSS5-OSS6. For each section, the standard deviation σ_b (0.082, 0.095 and 0.15 m for the four sections, respectively) and skewness S_k (-0.63, -0.38 and 0.71) are computed from the high-resolution topography data. These statistical moments reflect the overall evolution from small and compact coral colony over the reef crest, typically 20 cm-high, to much larger and spaced reef pinnacles standing on a smooth substratum partly covered by a thin layer of sand.

2.2 Data Processing

Pressure measurements were first corrected the atmospheric pressure measured ashore at the central island. The pressure timeseries were organised in 60-min bursts and converted into free surface elevation ζ using the nonlinear weakly dispersive reconstruction method described in Bonneton et al. (2018). Surface elevation energy spectra S at OSS sensors were computed using discrete Fourier transform on 409.2 s blocks overlapping by 75%. Statistical stability is increased by merging estimates over 5 frequencies (Elgar and Guza, 1985). This resulted in spectral estimates having approximately 96 equivalent degrees of freedom, with a spectral resolution of 0.0024 Hz. The energy balance analysis presented later on is performed over the 0.002-0.3 Hz frequency band, *i.e.* including both infragravity and short waves. Directional spectra at S4 are reconstructed from the measured near-bed collocated pressure/velocity data using the Bayesian Direct Method (Hashimoto, 1997). The analysis is performed over the full directional space with a 5^o directional resolution and focused in the short-wave (*i.e.* excluding infragravity motion) frequency range between 0.04 and 0.25 Hz (frequency resolution 0.001 Hz). Mean water levels (MWL) were computed for each 60-min burst. The unknown vertical position at S4 was adjusted assuming that, in the absence of waves, the sea level is flat, so that the difference between mean water levels measured at OSS6 and S4 shows a zero-intercept when plotted against the incident significant wave height.

2.3 Field Conditions

Figure 2A-C shows timeseries of wave characteristics at the forereef. The wave climate is typical of the south-west coast of Maupiti with long South Pacific swell waves, with a mean significant wave height of 1.9 m and a mean peak period about 13.5 s. The mean wave direction is 27^o in nautical convention, *i.e.* hitting the forereef with weak ($<$ 5^o) incidence during large wave events. Further refraction is expected to occur across the forereef (Sous et al., 2019), such that the assumption of a reef normal wave forcing at the reef crest is reasonable.

The MWL timeseries (Fig. 2D) shows the typical microtidal regime at Maupiti, with tide amplitude between 0.05 and 0.1 m. Mean water levels at the reef crest (blue line in Fig. 2D) show a systematic overheight related to the wave setup generated by intense wave breaking over the forereef. The wave setup also explains the systematic overheight of the lagoon MWL with respect to the open ocean (red line in Fig. 2D), classifying the Maupiti lagoon as a partly-closed system (Lindhart et al., 2021). The downward slope between reef crest and lagoon levels evolves following the spatial adjustment of the momentum balance (Sous et al., 2020a). The top of the reef crest colony has an elevation of 0.058 m, indicating that during the low water periods, the reef can submerged by less than 0.15 m of water. Cross-barrier current and transport (Fig. 2E) are systematically onshore-directed, ranging from 0 to 0.35 m/s and 0.42 m^2/s, respectively. They are principally controlled by the incident wave energy (Sous et al., 2017,0): the larger the waves, the stronger the cross-barrier barotropic pressure gradient, the stronger the current is.

3 Theoretical Framework

When averaged over many wave cycles, the cross-barrier evolution of the wave energy flux results from the combined effects of wave breaking, frictional dissipation and nonlinear energy transfers. Since we here focus on the frictional energy dissipation, the analysis is performed over the reef flat area where wave breaking is absent, starting at the location corresponding to the OSS3 sensor (Fig. 1).

Because of the presence of currents, the wave action balance is considered instead of the wave energy balance. For each frequency component j of absolute frequency f_j,

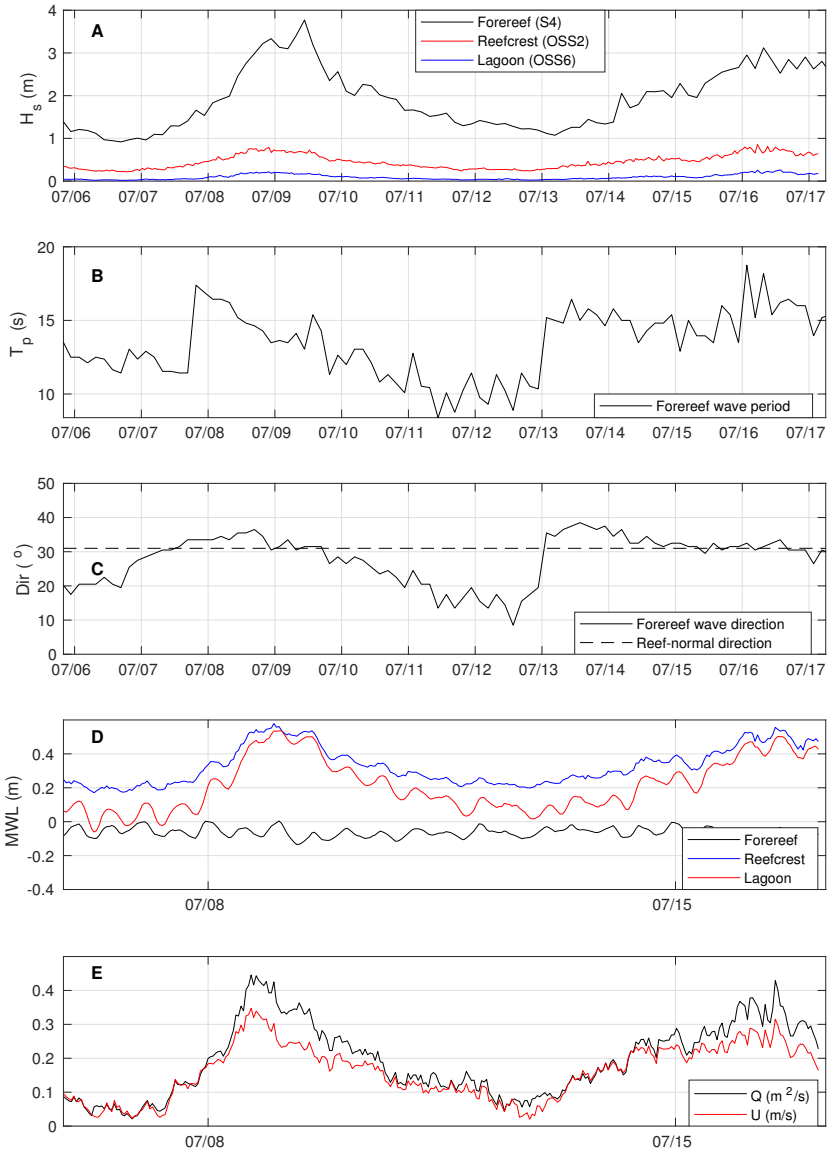

Figure 2. Overview of hydrodynamic conditions observed during the field experiment. A, B, C: SW significant wave height (computed as $4\sqrt{m_0}$, with m_0 being the zeroth moment of ζ computed over the SW frequency band) at S4 (forereef), OSS3 and OSS5, and peak period and peak direction at S4. D: Mean Water Level at S4 (forereef), OSS2 (reef crest) and OSS6 (lagoon). E: cross-barrier transport and depth-averaged current estimated at the reef crest.

the wave action is defined as $N_j = E_j/\sigma_j$, where E_j is the wave energy and σ_j the intrinsic radial frequency (*i.e.* defined in the frame of reference moving with the current). E_j is approximated with linear theory as $E_j = 0.5\rho g a_j^2$ where the wave amplitude is computed from the free surface elevation density spectrum S as $a_j = \sqrt{2S_j\Delta f}$, with Δf the frequency resolution. The intrinsic radial frequency σ_j (and wave number k_j) are obtained from the linear dispersion relationship including the Doppler shift, *i.e.*

$$\sigma_j^2 = (2\pi f_j - k_j U)^2 = g k_j \tanh(k_j D), \tag{1}$$

where U is the current magnitude in the direction of wave propagation (positive landwards) and D the local mean water depth (still water depth plus setup/down).

To estimate the frequency-dependant dissipation, we follow a similar approach as Chawla and Kirby (2002) and evaluate the action balance for each frequency bin (centered around frequency f_j). Mainly forced by large remotely-generated low pressure systems in the austral ocean, the wave field is assumed to be stationary over the considered 60-min time periods. Further assuming no breaking and a 1D problem (both waves and currents are in the cross-barrier direction), the wave action balance writes

$$\frac{\partial}{\partial x} C_{g,j} N_j = \frac{1}{\sigma_j}\left(-\epsilon_{f,j} + S_{nl,j}\right) \tag{2}$$

where $\epsilon_{f,j}$ is the energy dissipated through friction and $S_{nl,j}$ corresponds to nonlinear energy transfers between triads of frequencies. In this expression, $C_{g,j}$ is the absolute group velocity (defined in a fixed frame reference), given by linear wave theory as:

$$C_{g,j} = \frac{1}{2}\left(1 + \frac{2k_j D}{\sinh(2k_j D)}\right)\frac{\sigma_j}{k_j} + U. \tag{3}$$

To estimate the spatially averaged frictional dissipation $\langle \epsilon_{f,j} \rangle$ between each pair of adjacent sensors (called s_1-s_2 in the following), Equation 2 is discretized as:

$$\left\langle \frac{\epsilon_{f,j}}{\sigma_j} \right\rangle = \left\langle \frac{S_{nl,j}}{\sigma_j} \right\rangle - \frac{\Delta F_j}{\Delta x}, \tag{4}$$

where $\Delta x = x^{s_2} - x^{s_1}$ is the distance separating the sensors, $\Delta F_j = F_j^{s_2} - F_j^{s_1}$ is the difference in action flux between sensors ($F_j = C_{g,j} N_j$). The angle brackets indicate spatial averaging, *i.e.* $\langle \cdot \rangle = \frac{1}{\Delta x}\int_{x^{s_1}}^{x^{s_2}} \cdot \, dx$.

3.1 Nonlinear Transfers

The spatially averaged triad source term $\langle S_{nl,j} \rangle$ is approximated as the average of its values at the adjacent sensors s_1 and s_2, *i.e.*

$$\left\langle \frac{S_{nl,j}}{\sigma_j} \right\rangle \approx \frac{1}{2}\left(\left.\frac{S_{nl,j}}{\sigma_j}\right|_{s_1} + \left.\frac{S_{nl,j}}{\sigma_j}\right|_{s_2} \right).$$

At each sensor, the nonlinear transfers of energy between triads of frequencies are modelled with the Boussinesq theory of Herbers et al. (2000):

$$S_{nl,j} = \rho g \frac{3\pi f}{D} \sum_{m=-\infty}^{m=\infty} \Im\left\{ B_{m,j-m}^* \right\} \tag{5}$$

where B is the bispectrum of the free surface elevation computed after Kim and Powers (1979), $\Im\{\cdot\}$ refers to the imaginary part and $*$ denotes the complex conjugate. The Boussinesq approximation of S_{nl} was derived assuming that the wave field is weakly nonlinear, weakly dispersive, and that these effects are of similar order (Herbers and Burton, 1997).

As explained in Martins et al. (2021), Eq. 5 differs from the expression of Herbers et al. (2000) (their Eq. 2) in several points: the conjugate of B is taken in order to be consistent with their definition of the bispectrum (conjugate of the present definition), and we here retain the full integral formulation as originally given by Herbers and Burton (1997). Bispectra of ζ are computed using the same parameters than surface elevation energy spectra described in Section 2.2.

3.2 Bottom Friction

The spatially averaged frictional dissipation $\langle \epsilon_{f,j} \rangle$, obtained from Equation 4, is compared to the parameterization proposed by Madsen et al. (1989) and Madsen (1995) (see also Lowe et al., 2005, in the coral reef context) where $\epsilon_{f,j}$ can be expressed as:

$$\epsilon_{f,j} = \frac{1}{4} \rho f_{e,j} u_{b,r} u_{b,j}^2 \tag{6}$$

with $f_{e,j}$ the wave energy dissipation factor, $u_{b,j}$ the near-bed velocity given by $u_{b,j} = 2\pi f_j / \sinh(k_j D)$. $u_{b,r}$ is a representative maximum near-bed velocity defined as:

$$u_{b,r} = \sqrt{\sum_{j=1}^{N} u_{b,j}^2} \tag{7}$$

$f_{e,j}$ is then inferred combining Eqs. 4 (dissipation estimated from the measured flux) and 6 (dissipation predicted by the parameterization of Madsen (1995)):

$$f_{e,j} = \frac{\left\langle \frac{S_{nl,j}}{\sigma_j} \right\rangle - \frac{\Delta F_j}{\Delta x}}{\frac{1}{4} \left\langle \frac{\rho}{\sigma_j} u_{b,r} u_{b,j}^2 \right\rangle} \tag{8}$$

Note that the discretization approach used here relies on the calculation of energy flux at the sensors while the spatially-averaged terms in Equation 8 are evaluated at mid-point, i.e. the denominator is estimated as $\frac{1}{8}\rho((\frac{u_{br}, u_{b,j}^2}{\sigma_j})_{i+1} + (\frac{u_{br}, u_{b,j}^2}{\sigma_j})_i)$, where i and $i+1$ denote two successive sensors. The wave energy dissipation factor $f_{e,j}$ is related to the wave friction factor $f_{w,j}$ by accounting for the phase lag between bottom shear stress and near-bed horizontal velocity (Madsen, 1995; Lowe et al., 2005). Note that the phase lag effect on the friction factor is weak (less than 5%) for the considered conditions. The representative wave friction factor $f_{w,r}$ is defined as:

$$f_{w,r} = \frac{f_{e,r}}{\cos \Phi_r} \tag{9}$$

where $\cos \Phi_r$ is the representative phase angle and $f_{e,r}$ is the representative energy dissipation factor given by:

$$f_{e,r} = \frac{\sqrt{\sum_{j=1}^{N} f_{e,j} u_{b,j}^2}}{\sqrt{\sum_{j=1}^{N} u_{b,j}^2}} \tag{10}$$

The j-th wave friction factor is finally given by:

$$f_{w,j} = \left(\frac{f_{e,j}}{\sqrt{f_{w,r}} \cos \Phi_j} \right)^2 \tag{11}$$

Classical parameterizations from rough turbulent wave boundary layers (Madsen, 1995) define the wave friction factor as a function of the ratio of the near-bed horizontal wave orbital excursion $A_b = \frac{u_{b,r}}{\omega_j}$ to a hydraulic roughness height k_r (Swart, 1974; Madsen, 1995):

$$f_{w,j} = C_\mu \exp\left(a_1 \left(\frac{C_\mu u_{b,r}}{k_r \omega_j} \right)^{a_2} + a_3 \right) \tag{12}$$

The C_μ factor is used to account for the additional role played by the current in wave energy dissipation Madsen (1995). In the present case where waves and current directions are aligned, C_μ can be written:

$$C_\mu = \left(1 + 2\mu + \mu^2\right)^{1/2} \tag{13}$$

where μ is the ratio of current and wave bottom shear stress. C_μ is equal to 1 in the absence of current. The current shear stress is here deduced from the log depth-dependent formulation of friction coefficient provided by Sous et al. (2022), able to cover the full range of depth conditions observed at each section of the barrier reef flat.

Different values have been proposed for the constants a_1, a_2 and a_3 (Nielsen, 1992; Madsen, 1995), leading to variability in f_w predictions at small ranges of A_b/k_r (typically < 10). The values 5, 0.15 and -5.9 are used here, based on the optimized agreement for both the present data and other studies displayed in Figure 4B. For each section, the model is then locally fitted on the data using k_r as RMSE-optimizing parameter.

Finally, in order to ease comparison with Madsen's formulation, and in particular to compare the dependency of wave friction coefficients on A_b/k_r and C_μ, the experimental $f_{w,j}$ dataset is averaged on both A_b/k_r and C_μ bins.

4 Results

Figures 3A,B,C depicts the relationship between the numerator and the denominator of Eq. 8. The non-linearity and the spread of the relationship reflects the variability of the spectral wave friction factor $f_{e,j}$ depending on local wave features, depth and current intensity. Finer insight on $f_{e,j}$ is provided by Figures 3D-I which depict the relationship between the spectral wave friction coefficient $f_{w,j}$ and the A_b/k_r ratio, with color levels indicating the C_μ values. The observed wave friction coefficients are in the typical range of observations on coral reefs in the field (Péquignet et al., 2011; Lowe et al., 2005; Monismith et al., 2013,0; Acevedo-Ramirez et al., 2021). As expected, the friction factor increases with decreasing A_b/k_r. The current-induced shear increase is mainly visible for $A_b/k_r > 3$, while at smaller A_b/k_r friction factors appears nearly independent of C_μ. The current effect is less straightforward for the far back-reef (OSS5-OSS6) where the currents are weaker due to larger depth. The increased discrepancy between field measurements and theoretical predictions observed at OSS3-OSS4 for strong current and large A_b/k_r may be related to changes in the boundary layer dynamics but this remains difficult to interpret with the present dataset.

A comparison is performed between the measured friction factor (Eq. 8) and the value inferred from the spectral wave-current model (Eq. 12). The best-fit k_r values obtained are 0.35, 0.39 and 0.73m for the three reef sections. A satisfactory agreement is obtained with existing parameterization (Madsen, 1995), based on the assumption that the bed roughness can be represented by a single length scale, the hydraulic roughness k_r, presumably related to the statistics of seabed topography. In particular, the parameterization is observed to perform quite well even for small range of A_b/k_r reached over OSS3-OSS4 and OSS4-OSS5 sections. A first statistical relationship can be estimated between k_r and the standard deviation of the bed elevation around $k_r = 4\sigma_b$ (see Figure 4A). While more data points would have been necessary to provide a definitive conclusion, the increased k_r/σ_b ratio for OSS5-OSS6 may indicate that frictional dissipation may not only involve the bed roughness standard deviation as bed geometry control factor. Considering the large spread of k_r/σ_b relationship reported from in situ data (Gon et al., 2020), recent studies of wave dissipation over rough bottom attempted to establish a direct empirical relationship between the SW-frequency-integrated energy dissipation factor f_e and the A_b/σ_b ratio. Such an approach discards the theoretical framework from Madsen (1995) to focus on an empirical parameterization, following Soulsby

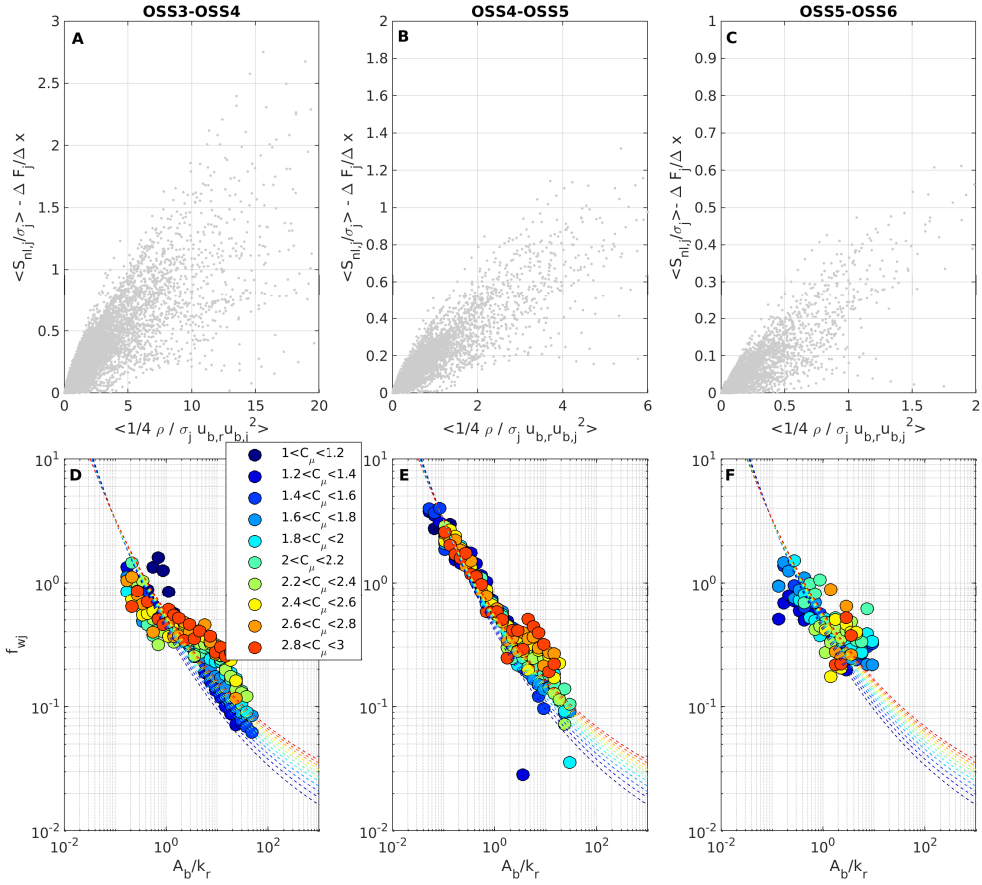

Figure 3. Top: Dissipation estimated from the observed action flux gradient $\langle \epsilon_{f,j}/\sigma_j \rangle = \langle S_{nl,j}/\sigma_j \rangle - \Delta F_j/\Delta x$ as a function of $\langle \epsilon_{f,j}/\sigma_j \rangle / f_{e,j} = 1/4 \langle \rho/\sigma_j u_{b,r} u_{b,j}^2 \rangle$ according to Madsen (1995)'s parameterization over OSS3-OSS4, OSS4-OSS5 and OSS5-OSS6 barrier sections. Bottom: Wave friction factor $f_{w,j}$ vs the ratio between near-bed wave excursion A_b and bed roughness k_r for the binned field data (colored circles) and the predictions from Madsen's formulation (Madsen, 1995) (dashed lines). The color levels refer to the value of C_μ factor.

(1997), which assumes that σ_b could be a single, unique metric of bed roughness. 4B compiles a series of recent dataset on rocky (Poate et al., 2016; Gon et al., 2020) and coral (Lowe et al., 2005; Lentz et al., 2016) environments. The coral reef data of Rogers et al. (2016) is also displayed, assuming that $k_r = 4\sigma_b$. The present observations are included, integrating over the 0.04-0.3 Hz frequency band, restricting to weak current conditions $C_\mu < 1.2$ to remain comparable to other datasets and assuming that $f_e = f_w$ (Davis et al., 2020). The Maupiti data is well integrated in the global trend, showing a clear increase of the friction coefficient for decreasing A_b/σ_b. In particular, the data recovered on the compact coral portions of the Maupiti barrier (OSS3-OSS4 and OSS4-OSS5) are in good agreement with the observations performed over a coral reef platform in the Red Sea Lentz et al. (2016). The far back-reef (OSS5-OSS6) shows higher friction values, closer to the estimations performed by Gon et al. (2020) over a rocky shore in Monterey Bay.

5 Discussion

The present study provided a comprehensive analysis of the spectral wave friction factor over a roughness-varying section of the Maupiti reef barrier. The present observations combined with recent studies on rocky sites (see Gon et al., 2020, in Figure 4B) could suggest that, for a given standard deviation, seabeds with positively skewed distribution of elevation are prone to induce more wave dissipation than the normally- or negatively-skewed distribution seabeds, *i.e.* high protruding relief features induce more dissipation than deep crevasses. While further dedicated observations are required to draw more robust conclusion, this observation may question the validity of the underlying assumption that a single length scale (σ_b in Figure 4) can represent the morphological complexity of real seabeds, in line with numerous observations performed on uniform flow Chung et al. (2021). Further field and laboratory data, combining hydrodynamical and morphological measurements, need to be gathered to gain insight on the effect of the multi-scale roughness observed on most rocky and coral reefs, involving statistical distributions and spectra (Gon et al., 2020; Duvall et al., 2019; Sous et al., 2020b). In addition, the full 3D structure of the bed geometry, with potential in-canopy flow controlled by variable porosity, specific surface and tortuosity, will certainly act in differentiating coral reef and rocky seabeds, in particular in the case of large roughness. For A_b/σ_b of the order of 1 or less, one can expect that the bedform-induced perturbations largely exceed the typical height of the wave-current bottom boundary layer, leading to consider volume canopy-induced drag (Rosman and Hench, 2011; Sous et al., 2020a; Buckley et al., 2022) and inertial added-mass effects or, at the very least, not to consider the near-bed orbital velocity as the sole velocity scaling. In addition from the A_b/σ_b effect, the depth itself may affect the boundary layer dynamics when the relative submergence ratio is low. Part of the observed discrepancies between field data presented in Figure 4B may also be attributed to the definition of water depth, which is not straightforward in the presence of large roughness despite its major role in the energy balance and orbital amplitude calculation. This issue is directly related to the interpretation of terrain reliefs, necessarily split into bathymetry vs roughness. The approach proposed here followed the work of Sous et al. (2020b) based on the saturation regime observed in the spectrum of bed roughness may be retained for further studies. The present study is the first one to account for contributions of both non-linear transfers and current in the friction estimation. Depending on the studied site, this may affect the computation of friction factor and also explain part of the observed differences between sites. For Maupiti barrier reef, the averaged S_{nl} contribution on the $f_{w,j}$ estimation over the whole dataset is about 15 % while the contribution of current in the energy flux balance is approximately 9%.

Several parameterizations of the friction factor have been proposed in the literature (Grant and Madsen, 1982; Madsen, 1995; Nielsen, 1992; Soulsby, 1997). Figure 4B displays two main types of formulation: (i) the Madsen et al's approach (Madsen et al., 1989) with Maupiti-optimized set of coefficients and assuming that $k_r = 4\sigma_b$ and (ii) the Gon et al.'s approach (Gon et al., 2020) adapted from Soulsby (1997). Both approaches provide close predictions in the $0.3 < A_b/\sigma_b < 100$ range. At lower A_b/σ_b, the Madsen et al's parameterization (Madsen et al., 1989) tends to provide a better reproduction of field measurements, but these latters are still too sparse to draw robust conclusions. For $A_b/\sigma_b > 100$, the Gon et al.'s parameterization (Gon et al., 2020) is expected to underestimate the low roughness friction data previously reported (Nielsen, 1992; Lentz et al., 2016), which may lead to favor the Madsen et al's parameterization (Madsen et al., 1989). Note that the latter approach involves a set of four parameters (a_i and K_r) which add sensitivity to the data fitting. However, the selected set of values allows a good representation of both the present data and field observations at other sites, providing confidence in the proposed parameters.

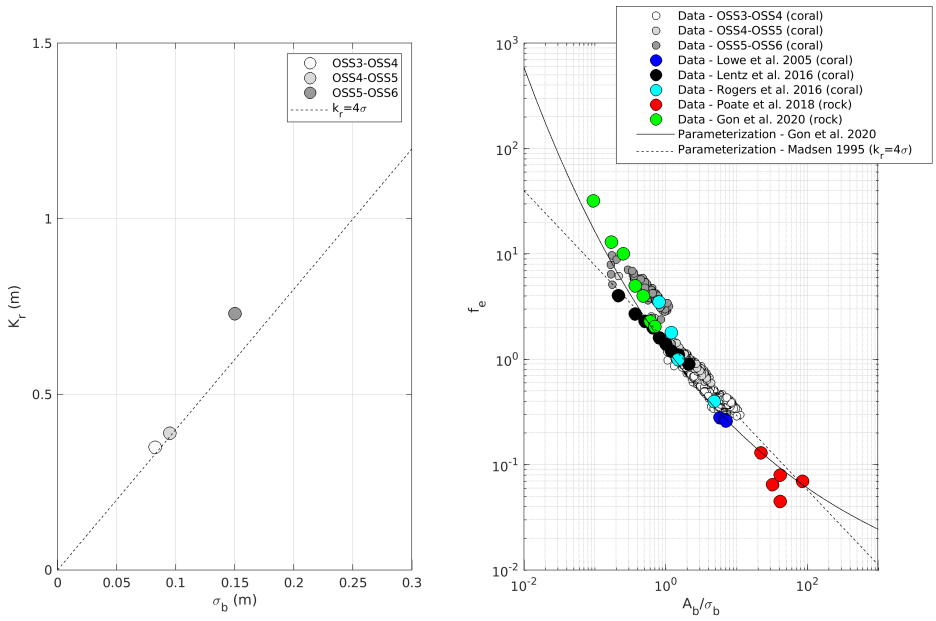

Figure 4. A: Hydraulic roughness K_r vs standard deviation of the bed elevation σ_r for the three zones of the Maupiti reef barrier. B: Frequency-integrated energy dissipation factor f_e vs near bed orbital amplitude to bed standard deviation ratio A_b/σ_b. Note that, for Rogers et al. (2016), representative points have been extracted from the complete forereef dataset.

6 Conclusion

Building on recent research efforts engaged to understand the interaction between wave and complex seabeds (Sambe et al., 2011; Lentz et al., 2016; Poate et al., 2016; Yu et al., 2018; Gon et al., 2020; Lavaud et al., 2022), the present study provides an unprecedented in situ validation of the frictional wave dissipation prediction by the wave-current boundary layer theory based on a full spectral analysis which allows to cover nearly three decades of A_b/σ_r. We isolate the contribution of frictional dissipation from breaking and non-linear energy transfers, account for the role of current and explore the relationship between hydrodynamics and seabed structure from fine topographical measurements. A modified version of the Madsen et al. (1989)'s parameterization is proposed. Using a simple relationship between the roughness height and the standard deviation of the bed elevation $k_r = 4\sigma_d$, the friction parameterization provide a correct overall prediction of friction factor for the present dataset and recent observations on coral and rocky reefs (Lowe et al., 2005; Lentz et al., 2016; Rogers et al., 2016; Gon et al., 2020; Poate et al., 2016). Further investigations are required to explore the role played by high-order statistical moments and other fine features of bed morphology on bed friction.

Data availability statement

The bottom pressure and bathymetric data used for the present study are available at https://doi.org/10.17882/91337

References

Acevedo-Ramirez, C. A., W. Stephenson, S. Wakes, and I. Mariño-Tapia (2021), Wave transformation on a fringing reef system with spur and groove structures, *Journal of Geophysical Research: Oceans*, *126*(9), e2020JC016,910.

Bonneton, P., D. Lannes, K. Martins, and H. Michallet (2018), A nonlinear weakly dispersive method for recovering the elevation of irrotational surface waves from pressure measurements, *Coastal Engineering*, *138*, 1–8, 10.1016/j.coastaleng.2018.04.005.

Buckley, M. L., R. J. Lowe, J. E. Hansen, A. R. van Dongeren, A. Pomeroy, C. D. Storlazzi, D. P. Rijnsdorp, R. F. da Silva, S. Contardo, and R. H. Green (2022), Wave-driven hydrodynamic processes over fringing reefs with varying slopes, depths, and roughness: Implications for coastal protection, *Journal of Geophysical Research: Oceans*, p. e2022JC018857, 10.1029/2022JC018857.

Chawla, A., and J. T. Kirby (2002), Monochromatic and random wave breaking at blocking points, *Journal of Geophysical Research: Oceans*, *107*(C7), 4–1.

Chung, D., N. Hutchins, M. P. Schultz, and K. A. Flack (2021), Predicting the drag of rough surfaces, *Annual Review of Fluid Mechanics*, *53*, 439–471.

Davis, K. A., G. Pawlak, and S. G. Monismith (2020), Turbulence and coral reefs, *Annual Review of Marine Science*, *13*.

Duvall, M. S., J. L. Hench, and J. H. Rosman (2019), Collapsing complexity: quantifying multi-scale properties of reef topography, *Journal of Geophysical Research: Oceans*, *124*, 5021–5038.

Elgar, S., and R. T. Guza (1985), Observations of bispectra of shoaling surface gravity waves, *Journal of Fluid Mechanics*, *161*, 425–448, 10.1017/S0022112085003007.

Gon, C. J., J. H. MacMahan, E. B. Thornton, and M. Denny (2020), Wave dissipation by bottom friction on the inner shelf of a rocky shore, *Journal of Geophysical Research: Oceans*, *125*(10), e2019JC015,963.

Gourlay, M. R., and G. Colleter (2005), Wave-generated flow on coral reefs—an analysis for two-dimensional horizontal reef-tops with steep faces, *Coastal Engineering*, *52*(4), 353–387.

Grant, W. D., and O. S. Madsen (1982), Movable bed roughness in unsteady oscillatory flow, *Journal of Geophysical Research: Oceans*, *87*(C1), 469–481.

Hashimoto, N. (1997), Analysis of the directional wave spectrum from field data, *Advances in coastal and ocean engineering*, *3*, 103–144.

Hearn, C. J. (1999), Wave-breaking hydrodynamics within coral reef systems and the effect of changing relative sea level, *Journal of Geophysical Research: Oceans (1978–2012)*, *104*(C12), 30,007–30,019.

Herbers, T. H. C., and M. C. Burton (1997), Nonlinear shoaling of directionally spread waves on a beach, *Journal of Geophysical Research: Oceans*, *102*(C9), 21,101–21,114, 10.1029/97JC01581.

Herbers, T. H. C., N. R. Russnogle, and S. Elgar (2000), Spectral energy balance of breaking waves within the surf zone, *Journal of Physical Oceanography*, *30*(11), 2723–2737.

Kim, Y. C., and E. J. Powers (1979), Digital Bispectral Analysis and Its Applications to Nonlinear Wave Interactions, *IEEE Transactions on Plasma Science*, *7*(2), 120–131, 10.1109/TPS.1979.4317207.

Lavaud, L., X. Bertin, K. Martins, M. Pezerat, T. Coulombier, and D. Dausse (2022), Wave dissipation and mean circulation on a shore platform under storm wave conditions, *Journal of Geophysical Research: Earth Surface*, *127*(3), e2021JF006,466.

Lentz, S., J. Churchill, K. Davis, and J. Farrar (2016), Surface gravity wave transformation across a platform coral reef in the r ed s ea, *Journal of Geophysical Research: Oceans*, *121*(1), 693–705.

Lindhart, M., J. Rogers, S. Maticka, C. Woodson, and S. Monismith (2021), Wave modulation of flows on open and closed reefs, *Journal of Geophysical Research: Oceans*, *126*(4), e2020JC016,645.

Lowe, R. J., J. L. Falter, M. D. Bandet, G. Pawlak, M. J. Atkinson, S. G. Monismith, and J. R. Koseff (2005), Spectral wave dissipation over a barrier reef, *Journal of Geophysical Research: Oceans (1978–2012)*, *110*(C4).

Madsen, O. S. (1995), Spectral wave-current bottom boundary layer flows, in *Coastal Engineering 1994*, pp. 384–398.

Madsen, O. S., Y.-K. Poon, and H. C. Graber (1989), Spectral wave attenuation by bottom friction: Theory, in *Coastal Engineering 1988*, pp. 492–504.

Martins, K., P. Bonneton, and H. Michallet (2021), Dispersive characteristics of non-linear waves propagating and breaking over a mildly sloping laboratory beach, *Coastal Engineering*, *167*, 103,917, 10.1016/j.coastaleng.2021.103917.

Monismith, S. G., L. M. Herdman, S. Ahmerkamp, and J. L. Hench (2013), Wave transformation and wave-driven flow across a steep coral reef, *Journal of Physical Oceanography*, *43*(7), 1356–1379.

Monismith, S. G., J. S. Rogers, D. Koweek, and R. B. Dunbar (2015), Frictional wave dissipation on a remarkably rough reef, *Geophysical Research Letters*, *42*(10), 4063–4071.

Nielsen, P. (1992), *Coastal bottom boundary layers and sediment transport*, vol. 4, World scientific.

Péquignet, A.-C., J. Becker, M. Merrifield, and S. Boc (2011), The dissipation of wind wave energy across a fringing reef at ipan, guam, *Coral Reefs*, *30*(1), 71–82.

Poate, T., G. Masselink, M. Austin, M. Dickson, and P. Kench (2016), Observation of wave transformation on macro-tidal rocky platforms, *Journal of Coastal Research*, *75*, 602–606.

Qu, K., T. Liu, L. Chen, Y. Yao, S. Kraatz, J. Huang, G. Lan, and C. Jiang (2022), Study on transformation and runup processes of tsunami-like wave over permeable fringing reef using a nonhydrostatic numerical wave model, *Ocean Engineering*, *243*, 110,228.

Reidenbach, M. A., S. G. Monismith, J. R. Koseff, G. Yahel, and A. Genin (2006), Boundary layer turbulence and flow structure over a fringing coral reef, *Limnology and Oceanography*, *51*(5), 1956.

Rogers, J. S., S. G. Monismith, D. A. Koweek, and R. B. Dunbar (2016), Wave dynamics of a p acific a toll with high frictional effects, *Journal of Geophysical Research: Oceans*, *121*(1), 350–367.

Rogers, J. S., S. A. Maticka, V. Chirayath, C. B. Woodson, J. J. Alonso, and S. G. Monismith (2018), Connecting flow over complex terrain to hydrodynamic roughness on a coral reef, *Journal of Physical Oceanography*, *48*(7), 1567–1587.

Rosman, J. H., and J. L. Hench (2011), A framework for understanding drag parameterizations for coral reefs, *Journal of Geophysical Research: Oceans*, *116*(C8).

Sambe, A. N., D. Sous, F. Golay, P. Fraunié, and R. Marcer (2011), Numerical wave breaking with macro-roughness, *European Journal of Mechanics-B/Fluids*, *30*(6), 577–588.

Soulsby, R. (1997), Dynamics of marine sands: a manual for practical applications, *Oceanographic Literature Review*, *9*(44), 947.

Sous, D., C. Chevalier, J.-L. Devenon, J. Blanchot, and M. Pagano (2017), Circulation patterns in a channel reef-lagoon system, ouano lagoon, new caledonia, *Estuarine, Coastal and Shelf Science*, *196*, 315–330.

Sous, D., M. Tissier, V. Rey, J. Touboul, F. Bouchette, J.-L. Devenon, C. Chevalier, and J. Aucan (2019), Wave transformation over a barrier reef, *Continental Shelf Research*, *184*, 66–80.

Sous, D., G. Dodet, F. Bouchette, and M. Tissier (2020a), Momentum balance over a barrier reef, *Journal of Geophysical Research: Oceans*, *DOI:*

10.1029/2019JC015503.

Sous, D., F. Bouchette, E. Doerflinger, S. Meulé, R. Certain, G. Toulemonde, B. Dubarbier, and B. Salvat (2020b), On the small-scale fractal geometrical structure of a living coral reef barrier, *Earth Surface Processes and Landforms*, *45*(12), 3042–3054.

Sous, D., S. Maticka, S. Meulé, and F. Bouchette (2022), Bottom drag coefficient on a shallow barrier reef, *Geophysical Research Letters*, *49*(6), e2021GL097,628.

Swart, D. H. (1974), Offshore sediment transport and equilibrium beach profiles.

Symonds, G., K. P. Black, and I. R. Young (1995), Wave-driven flow over shallow reefs, *Journal of Geophysical Research: Oceans (1978–2012)*, *100*(C2), 2639–2648.

Yu, X., J. H. Rosman, and J. L. Hench (2018), Interaction of waves with idealized high-relief bottom roughness, *Journal of Geophysical Research: Oceans*, *123*(4), 3038–3059.